Check for updates

Enhancing the magneto-optical Kerr effect through the use of a plasmonic antenna

T. H. J. LOUGHRAN,* P. S. KEATLEY, E. HENDRY, W. L. BARNES, AND R. J. HICKEN

University of Exeter, Department of Physics and Astronomy, Exeter, EX4 4QL, UK
t.h.j.loughran@ex.ac.uk

Abstract: We employ an extended finite-element model as a design tool capable of incorporating the interaction between plasmonic antennas and magneto-optical effects, specifically the magneto-optical Kerr effect (MOKE). We first test our model in the absence of an antenna and show that for a semi-infinite thin-film, good agreement is obtained between our finite-element model and analytical calculations. The addition of a plasmonic antenna is shown to yield a wavelength dependent enhancement of the MOKE. The antenna geometry and its separation from the magnetic material are found to impact the strength of the observed MOKE signal, as well as the antenna's resonance wavelength. Through optimization of these parameters we achieved a MOKE enhancement of more than 100 when compared to a magnetic film alone. These initial results show that our modeling methodology offers a tool to guide the future fabrication of hybrid plasmonic magneto-optical devices and plasmonic antennas for magneto-optical sensing.

References and links

1. J. Kerr, "On rotation of the plane of polarization by reflection from the pole of a magnet," London, Edinburgh, Dublin Philosophical Mag. J. Sci. **3**, 321–343 (1877).
2. J. Kerr, "On reflection of polarized light from the equatorial surface of a magnet," London, Edinburgh, Dublin Philosophical Mag. J. Sci. **5**, 161–177 (1878).
3. S. D. Bader and J. L. Erskine, "Magneto-Optical Effects," in *Ultrathin Magnetic Structures II*, B. Heinrich and J. A. C. Bland, eds. (Springer, 1994), pp. 287–303.
4. M. Mansuripur, *The Physical Principles of Magneto-optical Recording* (Cambridge University Press, 1995).
5. A. Hubert and R. Schäfer, "Domain Observation Techniques," in *Magnetic Domains* (Springer,1998)
6. Q. Qiu and S. D. Bader, "Surface magneto-optic Kerr effect," Rev. Sci. Instrum. **71**, 1243–1255 (2000)
7. P. Ma and P. R. Norton, "Growth of ultrathin Fe films on Ge(100): Structure and magnetic properties," Phys. Rev. B. **56**, 9881–9886 (1997)
8. D. Kumar, P. Gupta, and A. Gupta, "*In situ* surface magneto-optical Kerr effect (s-MOKE) study of ultrathin soft magnetic FeCuNbSiB alloy films," Mater. Res. Express, **1**, 046405 (2014)
9. P. S. Keatley, V. V. Kruglyak, R. J. Hicken, J. R. Childress, and J. Katine, "Acquisition of vector hysteresis loops from micro-arrays of nano-magnets," J. Magn. Magn. Mater. **306**, 298–301 (2006).
10. M. R. Freeman, and J. F. Smyth, "Picosecond time-resolved magnetization dynamics of thin-film heads," J. Appl. Phys. **79**, 5895–5900 (1996)
11. W. K. Hiebert, A. Stankiewicz, and M. R. Freeman, "Direct Observation of Magnetic Relaxation in a Small Permalloy Disk by Time-Resolved Scanning Kerr Microscopy," Phys. Rev. Lett. **79**, 1134–1137 (1997)
12. Th. Gerrits, H. A. M. van den Berg, J. Hohlfeld, L. Bär, and Th. Rasing, "Ultrafast precessional magnetization reversal by picosecond magnetic field pulse shaping," Nature **418**, 509–512 (2002)
13. R. A. J. Valkass, W. Yu, L. R. Shelford, P. S. Keatley, T. H. J. Loughran, R. J. Hicken, S. A. Cavill, G. van der Laan, S. S. Dhesi, M. A. Bashir, M. A. Gubbins, P. J. Czoschke, and R. Lopusnik, "Imaging the equilibrium state and magnetization dynamics of partially built hard disk write heads," Appl. Phys. Lett. **106**, 232404 (2015).
14. P. S. Keatley, V. V. Kruglyak, A. Neudert, M. Delchini, R. J. Hicken, J. R. Childress, and J. A. Katine, "Time and vector-resolved magneto-optical kerr effect measurements of large angle precessional reorientation in a 2x2um ferromagnet," J. Appl. Phys. **105**, 07D308 (2009).
15. P. S. Keatley, S. R. Sani, G. Hrkac, S. M. Mohseni, P. Dürrenfeld, T. H. J. Loughran, J. Åkerman, and R. J. Hicken, "Direct observation of magnetization dynamics generated by nanocontact spin-torque vortex oscillators," Phys. Rev. B **94**, 060402 (2016).

16. W. Yu, P. Gangmei, P. S. Keatley, R. J. Hicken, M. A. Gubbins, P. J. Czoschke, and R. Lopusnik, "Time resolved scanning Kerr microscopy of hard disk writer structures with a multilayered yoke," Appl. Phys. Lett. **102**, 162407 (2013).
17. D. K. Gramotnev and S. I. Bozhevolnyi, "Plasmonics beyond the diffraction limit," Nat. Photonics **4**, 83–91 (2010).
18. T. W. Ebbesen, H. J. Lezec, T. Ghaemi, and P. A. Wolff, "Extraordinary optical transmission through sub-wavelength hole arrays," Nature **391**, 667–669 (1998).
19. C. Genet and T. W. Ebbesen, "Light in tiny holes," Nature **445**, 39–46 (2007).
20. O. Mahboub, S. Carretero-Palacios, C. Genet, F. J. Garcia-Vidal, S. G. Rodrigo, L. Martin-Moreno, and T. W. Ebbesen, "Optimization of bull's eye structures for transmission enhancement," Opt. Express **18**, 11292–11299 (2010).
21. S. Carretero-Palacios, O. Mahboub, F. J. Garcia-Vidal, L. Martin-Moreno, S. G. Rodrigo, C. Genet, and T. W. Ebbesen, "Mechanisms for extraordinary optical transmission through bull's eye structures," Opt. Express **19**, 10429–10442 (2011).
22. M. Fleischmann, P. Hendra, and A. McQuillan, "Raman spectra of pyridine adsorbed at a silver electrode," Chem. Phys. Lett. **26**, 163–166 (1974).
23. F. Festy, A. Demming, and D. Richards, "Resonant excitation of tip plasmons for tip-enhanced raman snom," Ultramicroscopy **100**, 437 – 441 (2004).
24. B. Hecht, B. Sick, U. P. Wild, V. Deckert, R. Zenobi, O. J. F. Martin, and D. W. Pohl, "Scanning near-field optical microscopy with aperture probes: Fundamentals and applications," J. Chem. Phys. **112**, 7761–7774 (2000).
25. R. G. Milner and D. Richards, "The role of tip plasmons in near-field raman microscopy," J. Microsc. **202**, 66–71 (2001).
26. S. B. Chaney, S. Shanmukh, R. A. Dluhy, and Y.-P. Zhao, "Aligned silver nanorod arrays produce high sensitivity surface-enhanced raman spectroscopy substrates," Appl. Phys. Lett. **87**, 031908 (2005).
27. S. Kawata, *Near-field Optics and Surface Plasmon Polaritons* (Springer, 2001).
28. P. Bharadwaj, B. Deutsch, and L. Novotny, "Optical antennas," Adv. Opt. Photonics **1**, 438–483 (2009).
29. P. Keatley, T. H. J. Loughran, E. Hendry, W. L. Barnes, R. J. Hicken, J. R. Childress, and J. A. Katine, "A platform for time-resolved scanning Kerr microscopy in the near-field," Rev. Sci. Instrum. **88**, 123708 (2017).
30. N. Maccaferri, A. Berger, S. Bonetti, V. Bonanni, M. Kataja, Q. H. Qin, S. van Dijken, Z. Pirzadeh, A. Dmitriev, J. Nogués, J. Åkerman, and P. Vavassori, "Tuning the magneto-optical response of nanosize ferromagnetic Ni disks using the phase of localized plasmons," Phys. Rev. Lett. **111**, 167401 (2013).
31. N. Maccaferri, J. B. González-Díaz, S. Bonetti, A. Berger, M. Kataja, S. van Dijken, J. Nogués, V. Bonanni, Z. Pirzadeh, A. Dmitriev, J. Åkerman and P. Vavassori, "Polarizability and magnetoplasmonic properties of magnetic general ellipsoids,", Opt. Express **21**, 9875–9889 (2013).
32. N. Maccaferri, K. E. Gregorczyk, T. V. A. G. de Oliveira, M. Kataja, S. van Dijken, Z. Pirzadeh, A. Dmitriev, J. Åkerman, M. Knez, and P. Vavassori, "Ultrasensitive and label-free molecular-level detection enabled by light phase control in magnetoplasmonic nanoantennas," Nat. Commun. **6**, 6150 (2015).
33. A. Berger, R. A. de la Osa, A. Suszka, M. Pancaldi, J. Saiz, F. Moreno, H. Oepen, and P. Vavassori, "Enhanced magneto-optical edge excitation in nanoscale magnetic disks," Phys. Rev. Lett. **115**, 187403 (2015).
34. P. K. Jain, Y. Xiao, R. Walsworth, and A. E. Cohen, "Surface plasmon resonance enhanced magneto-optics (SuPREMO): Faraday rotation enhancement in gold-coated iron oxide nanocrystals," Nano Lett. **9**, 1644–1650 (2009).
35. J. B. González-Díaz, A. García-Martín, J. M. García-Martín, A. Cebollada, G. Armelles, B. Sepúlveda, Y. Alaverdyan, and Mikael Käll, "Plasmonic Au/Co/Au Nanosandwiches with Enhanced Magneto-optical Activity," Small **4** 202–205 (2008).
36. G. Armelles, J. B. González-Díaz, A. García-Martín, J. Miguel García-Martín, A. Cebollada, M. Ujué González, S. Acimovic, J. Cesario, R. Quidant, and G. Badenes, "Localized surface plasmon resonance effects on the magneto-optical activity of continuous Au/Co/Au trilayers," Opt. Express **16** 16104–16112 (2008).
37. J. Zak, E. Moog, C. Liu, and S. Bader, "Fundamental magnetooptics," J. Appl. Phys. **68**, 4203-4207 (1990).
38. G. Neuber, R. Rauer, J. Kunze, T. Korn, C. Pels, G. Meier, U. Merkt, J. Bäckström, and M. Rübhausen, "Temperature-dependent spectral generalized magneto-optical ellipsometry," Appl. Phys. Lett. **83**, 4509–4511 (2003).
39. J. Wu, J. R. Moore, and R. Hicken, "Optical pump-probe studies of the rise and damping of ferromagnetic resonance oscillations in a thin fe film," J. Magn. Magn. Mater. **222**, 189–198 (2000).
40. P. B. Johnson and R. W. Christy, "Optical constants of the noble metals," Phys. Rev. B **6**, 4370–4379 (1972).
41. R. Atkinson and P. H. Lissberger, "Sign conventions in magneto-optical calculations and measurements," Appl. Opt. **31**, 6076–6081 (1992).
42. W. Yu, P. S. Keatley, P. Gangmei, M. K. Marcham, T. H. J. Loughran, R. J. Hicken, S. A. Cavill, G. van der Laan, J. R. Childress, and J. A. Katine, "Observation of vortex dynamics in arrays of nanomagnets," Phys. Rev. B **91**, 174425 (2015).
43. M. A. Garcia, "Surface plasmons in metallic nanoparticles: fundamentals and applications," J. Phys. D: Appl. Phys. **44**, 1–20 (2011).

1. Introduction

The magneto-optical Kerr effect (MOKE), discovered by John Kerr in 1877 [1, 2], describes the change in polarisation state of light when reflected from a magnetic material. When s or p polarised light is incident upon a magnetic material a rotation and change in ellipticity may be induced upon the reflected beam. In general the effect can be thought of as the combination of contributions from three separate geometries, known as the "polar", "longitudinal" and "transverse" MOKE [3]. The geometries are defined by the direction of the magnetization within the material relative to the plane of incidence of the light wave as shown in Fig. 1.
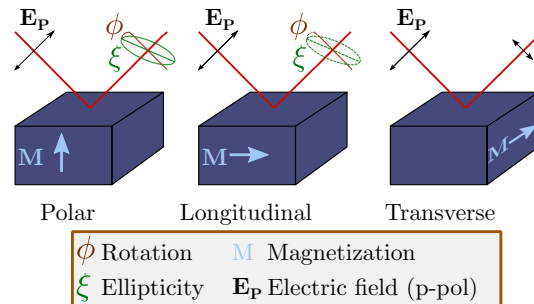

Fig. 1. Schematic of the various MOKE geometries. The single ended arrow indicates the direction of the magnetization in each case. The incident optical beam is assumed to be p-polarized. The transverse MOKE configuration produces no change in polarization state, but instead modifies the amplitude of the reflected electric field.

Polar MOKE has been used in magneto-optical recording [4], although this technology has now been largely superseded. The polar, longitudinal and transverse MOKE effects have been exploited in magnetometry and imaging measurements performed upon magnetic thin films [3,5,6]. MOKE is particularly favoured for the non-invasive evaluation of samples and devices that are spatially inhomogeneous, and for in-situ measurements within growth chambers [7, 8]. The MOKE can be used to directly image the surface magnetisation of a magnetic thin film, with all components of the vector magnetisation being resolved through the use of a suitable detector [9]. The additional use of an ultrafast laser source allows high frequency magnetisation dynamics to be probed and imaged [10–16]. The principal limitation of the magneto-optical probe is the finite spatial resolution associated with the optical diffraction limit. However, plasmonics may hold the key to bypassing this restriction. Plasmonics is a broad field concerned with the interaction of electromagnetic radiation with mainly metallic structures [17]. Of particular interest here is the near field region of a plasmonic structure, which can support a localised plasmon mode. Indeed it is well known that plasmonic excitations have the ability to concentrate electromagnetic fields within a strongly sub-wavelength region [17–21]. This field confinement and enhancement has been used to enhance local interactions, for example in surface enhanced Raman spectroscopy (SERS) [22–26], whilst a variety of combinations of plasmonic near field effects and imaging protocols have also been explored. [27, 28]. The combination of plasmonic enhancement with magneto-optical effects has recently come into focus, largely driven by the need for non-invasive optical imaging of magnetic structures with sub-diffraction-limited spatial resolution [29]. However most recent work has concentrated on the excitation of plasmonic modes within magnetic materials [30–33]. Ferromagnetic metals are generally poor media for the excitation of plasmonic modes, while most low-loss plasmonic materials do not exhibit magnetic properties other than diamagnetism. However it has been shown that magneto-optical effects can be enhanced by coating magnetic nano-particles with gold [34], or by creating multi-layer Au/Co/Au nano-particles [35] or gold nano-particles held above a Au/Co/Au film by means of a

dielectric spacer [36]. In the present work, our aim is to use finite element modeling to explore the effect of placing a plasmonic device close to, but physically separate from, a magnetic material. This geometry is particularly desirable since it may facilitate the probing of planar magnetic structures of arbitrary geometry and magnetization state through modification of the tips used in a recently developed magneto optical near field imaging tool [29]. It provides opportunities to maximize plasmonic enhancement without directly affecting the magnetic properties of the system under investigation. In the following sections a finite element model is described that can be used to resolve magneto-optical effects in both simple and complex magnetic structures. Details of this flexible model are presented, and illustrated by application to a simple gold nano-disc antenna. The rotation and ellipticity arising from both the polar and longitudinal MOKE are calculated for a continuous film and shown to be consistent with analytical theory. When a plasmonic gold nano-disc structure is placed close to the film, the MOKE response is found to be enhanced by up to two orders of magnitude. Finally the nature of this enhancement is discussed along with its potential application as a resonant plasmonic probe.

2. Modelling the MOKE

The practical realisation of a plasmonic antenna for near field magneto-optical measurements requires the plasmonic element to be separate from the magnetic material. The complexity of a plasmonic antenna interacting with a magnetic material is such that traditional mathematical approaches are not viable, especially for antenna structures of non trivial geometry. However the use of a suitable finite element modelling program allows arbitrarily complex structures to be modelled. Here finite element modelling was performed using the commercial software package "COMSOL Multiphysics" (from hereon referred to as "COMSOL"). This software was chosen so as to allow user definition of the permittivity as a complex non-Hermitian tensor, which is necessary for the description of magneto-optical effects. We define the total permittivity of the magnetic layer ϵ_{MO} as a complex tensor as in [5] Hubert and Schäfer and presented elsewhere [6, 37],

$$\epsilon_{MO} = \epsilon_0 \epsilon_r \begin{bmatrix} 1 & iB_zQ & -iB_yQ \\ -iB_zQ & 1 & iB_xQ \\ iB_yQ & -iB_xQ & 1 \end{bmatrix}, \tag{1}$$

where ϵ_0 is the permittivity of free space. Here ϵ_r is the relative permittivity of the material in the absence of magnetization, and is generally complex and frequency dependent for any metallic magnetic material. B_i is the direction cosine of the magnetization along the ith axis, and Q is the complex Voigt constant (a property of the specific magnetic material). Since the primary focus of the present study was the wavelength dependent magneto-optical response associated with the geometry of a plasmonic element, ϵ_{MO} was treated as being independent of frequency/wavelength. For the models presented here, we assume values typical of permalloy when illuminated by light of 800nm incident wavelength, obtained from reference [38], giving an index of $n = 2.25 + i3.7$ and Voigt constant of $Q = 0.006 - i0.011$. In [39] Wu et al, the first order reflection coefficients for the interface between a non magnetic medium with refractive index n_0 and a magnetic medium of refractive index n_1 are given as

$$r_{ss} = \frac{n_0 \cos\theta_0 - n_1 \cos\theta_1}{n_0 \cos\theta_0 + n_1 \cos\theta_1} \tag{2}$$

$$r_{pp} = \frac{n_1 \cos\theta_0 - n_0 \cos\theta_1}{n_1 \cos\theta_0 + n_0 \cos\theta_1} + \frac{2iQn_1n_0 \cos\theta_0 \sin\theta_1 B_y}{(n_1 \cos\theta_0 + n_0 \cos\theta_1)^2} \tag{3}$$

$$r_{ps} = -\frac{iQn_0n_1 \cos\theta_0 (\sin\theta_1 B_x - \cos\theta_1 B_z)}{\cos\theta_1 (n_0 \cos\theta_0 + n_1 \cos\theta_1)(n_1 \cos\theta_0 + n_0 \cos\theta_1)} \tag{4}$$

$$r_{sp} = \frac{iQn_0n_1 \cos\theta_0 (\sin\theta_1 B_x + \cos\theta_1 B_z)}{\cos\theta_1 (n_0 \cos\theta_0 + n_1 \cos\theta_1)(n_1 \cos\theta_0 + n_0 \cos\theta_1)} \qquad (5)$$

This analytical calculation assumes that field quantities vary in space and time as $exp(i(\mathbf{k} \cdot \mathbf{r} - \omega t))$, where $\mathbf{k}$ is the wave vector, $\mathbf{r}$ is the position vector, ω is the angular frequency, and t is the time. This form requires the imaginary part of the refractive index of the permalloy to have positive sign. With the p-polarized rotation ϕ_p and ellipticity ξ_p given as,

$$\phi_p = -Re\left\{\frac{r_{sp}}{r_{pp}}\right\} \qquad (6)$$

$$\xi_p = Im\left\{\frac{r_{sp}}{r_{pp}}\right\} \qquad (7)$$

For the above values, these analytical expressions for a semi-infinite slab of material predict values of Kerr rotation and ellipticity of 74.7 mDeg and −24.7 mDeg respectively, for normal incidence when the magnetization lies in the polar configuration as shown in Fig. 2. Plasmonic effects were later introduced by defining a frequency (wavelength) dependent complex permittivity for an adjacent gold nanostructure. This was accomplished by interpolating the gold permittivity data found in [40] Johnson et al, using the inbuilt linear interpolation algorithms found within COMSOL. The permittivity of the magnetic material was deliberately assumed to be independent of wavelength so as to allow the influence of the antenna upon the spectral response to be observed more clearly.
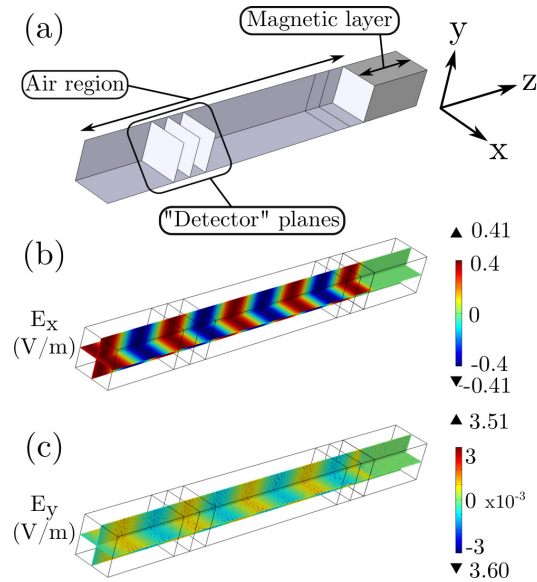

Fig. 2. Schematic of the periodic model geometry for calculation of the polar MOKE. (a) General schematic showing the magnetic region, air region, and slices through the model used in the recovery of the MOKE signal. (b) Model with the incident electric field polarization parallel to the $\hat{x}$ direction. (c) The $\hat{y}$ component of the electric field, which is the result of the magneto-optical rotation induced by the MOKE.

Since there are two self-consistent definitions of the complex permittivity arising from the choice of sign convention used in the description of wave propagation, this in turn leads to four possible sign conventions when describing the magneto optical permittivity (for greater insight

into the sign conventions used in describing magneto-optical permittivity, see reference [41]). In this work we chose signs of permittivity and Voigt constant such that we achieve agreement between finite element modeling and analytical calculation. This requires the permittivity and Voigt constant of the magnetic layer to be set equal to $\epsilon_{mag} = -8.628 - i16.50$ and $Q = -0.006 - i0.011$ respectively within COMSOL. Note that COMSOL assumes that field quantities vary as $exp(i(\omega t - \mathbf{k} \cdot \mathbf{r}))$, leading to the stated signs of the components of the permittivity.

The geometry for the simplest COMSOL model used is shown in Fig. 2. Here an incident plane wave lies normal to the surface of a planar magnetic layer (described by periodic boundary conditions in $\hat{x}$ and $\hat{y}$). Periodic boundary conditions minimized the physical geometry of the model, without compromising its accuracy. Therefore, the model represents an infinite array with the schematics showing just a single unit cell. The model shown has a unit cell, and hence period, of 200 nm in the $\hat{x}$ and $\hat{y}$ directions. In the present study the principal interest is the localized plasmonic mode associated with a nano-particle, that might be exploited within an antenna for near-field magneto-optical imaging, rather than resonances arising from a periodic structure. Therefore the period of the model was chosen to be smaller than the free space wavelength of any of the incident wavelengths used, in order to eliminate such artifacts and avoid diffracted modes. The incident electromagnetic wave was defined as a plane wave propagating towards the magnetic layer (in the $+\hat{z}$ direction in Fig. 2(b)), and linearly polarized along the $\hat{x}$ axis. The magnetization direction was defined to be out of plane, along the long $(-\hat{z})$ axis of the model, this corresponds to the polar MOKE geometry, shown in Fig. 1. While the choice of permalloy material properties with an out of plane magnetization may seem at odds with the in plane anisotropy typical of permalloy, it is not uncommon to measure the polar component of magnetization in measurements of precessional dynamics in permalloy structures [12, 42].The resulting reflected wave contains an additional electric field component in the $\hat{y}$ direction, shown in Fig. 2(c), due to the MOKE induced rotation and/or ellipticity. The complex field components were extracted through integration across one of the "detector" planes. From these field components, the MOKE rotation, ϕ and ellipticity, ξ were found using the formulae

$$\phi = \frac{(\mathrm{Re}E_x)(\mathrm{Re}E_y) + (\mathrm{Im}E_x)(\mathrm{Im}E_y)}{(\mathrm{Re}E_x)^2 + (\mathrm{Im}E_y)^2}, \tag{8}$$

$$\xi = \frac{(\mathrm{Re}E_x)(\mathrm{Im}E_y) - (\mathrm{Im}E_x)(\mathrm{Re}E_y)}{(\mathrm{Re}E_x)^2 + (\mathrm{Im}E_y)^2}, \tag{9}$$

that are valid for the small ϕ and ξ values commonly generated by the MOKE, and which assume the magnetic medium to be opaque and semi-infinite. Note that care must be taken with the meshing of the model to avoid inconsistencies between Kerr rotation values calculated at different detector planes. A mesh size of less than 40nm in the air region, with further refinement at the air/magnetic material interface, was found to produce minimal spatial variation of the observed Kerr signal. Initial polar MOKE modeling produced a Kerr rotation of 75 mDeg and ellipticity of −25 mDeg, with a variation between different models of ≈ 1 mDeg. These values are consistent with the values of 74.7 mDeg, and −24.7 mDeg calculated from analytical formulae. The longitudinal Kerr effect is expected to vanish at normal incidence, therefore modeling the effect requires the introduction of oblique incidence. This is non-trivial to introduce to periodic models, and therefore a different modeling geometry was required to model the longitudinal Kerr effect. This new geometry is shown in Fig. 3. This model also delivered reasonable agreement with analytical expressions for both polar and longitudinal MOKE over a large range of incidence angles, as shown in Fig. 4.
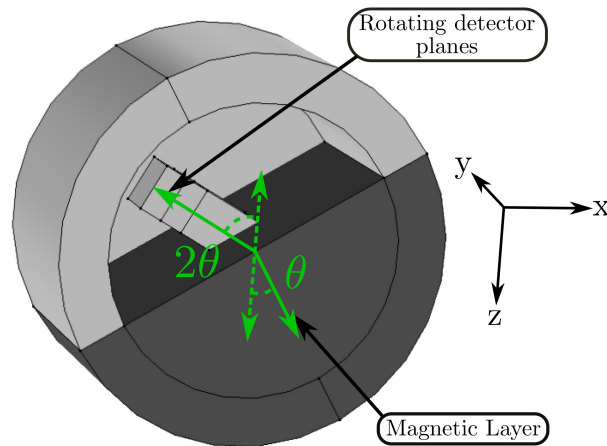
Fig. 3. Schematic of the non-periodic cylindrical model used for calculation of the MOKE signal for an arbitrary angle of incidence. The incident beam (not shown) propagates in the $\hat{z}$ direction, which is fixed. The detector plane and magnetic material rotate relative to the incident beam so as to maintain a standard θ 2θ geometry. As such the angle of incidence changes, while the geometry of the incident beam remains unaltered in COMSOL's coordinate system.
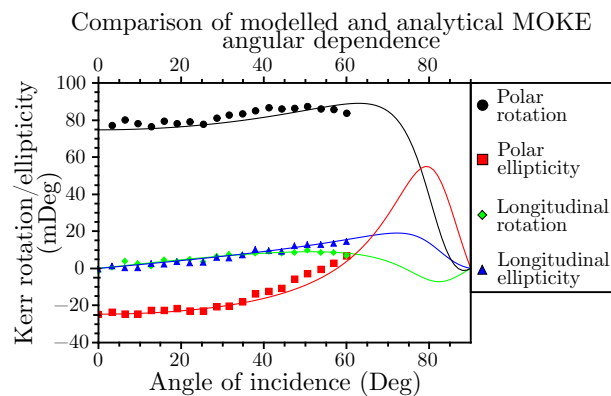

Fig. 4. Comparison of Kerr rotation/ellipticity values obtained from finite element modelling (data points) and analytical formulae (curves) for different angles of incidence. The finite element calculations were performed with the cylindrical model shown in Fig. 3. No data are shown for angles greater than 60° because at this point the detector plane enters the magnetic layer.

3. Modelling in the presence of a plasmonic antenna

The introduction of a gold nano-disc of 50 nm thickness into the normal incidence model, as shown in Fig. 5, yielded a wavelength-dependent enhancement of the MOKE. The dependence of the Kerr response upon wavelength is shown in Fig. 6. A fixed value of the magneto-optical constant corresponding to 800 nm wavelength was used for all calculations so that the wavelength-dependent response is due to the gold antenna rather than the magnetic film. Varying the diameter of the gold disc was found to shift the resonant wavelength of the system, as might be expected from previous work in which resonant wavelength of a plasmonic structure is found to vary with the size of the structure in question [36, 43]. However, the regime modeled here lies outside

the region of validity of reduced Mie scattering theory (due to particle shape), and the dipolar approximation due to particle size. Consequently, derivation of a fully analytical solution lies beyond the scope of the present paper.
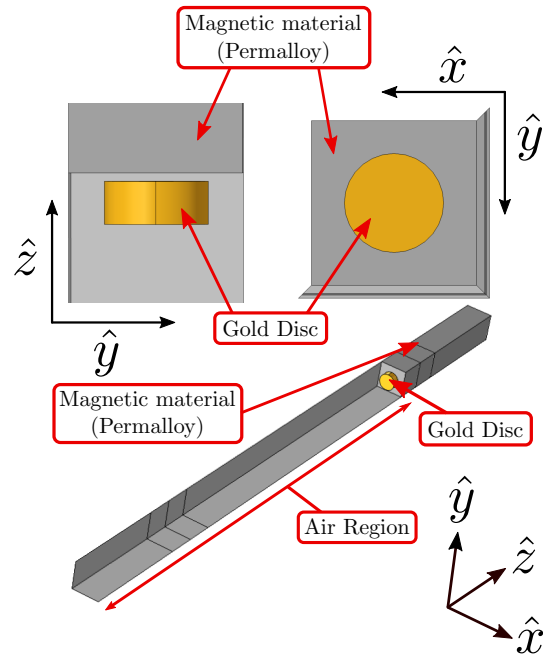

Fig. 5. Schematic of the periodic, model with addition of a gold nano-disc. A series of disc diameters were used, from 80 nm to 160 nm with the 100 nm diameter disc shown. The gold disc is separated from the magnetic material by a variable air gap (10 nm in this figure). The disc diameter was fixed at 50 nm for all modeling presented in this manuscript.
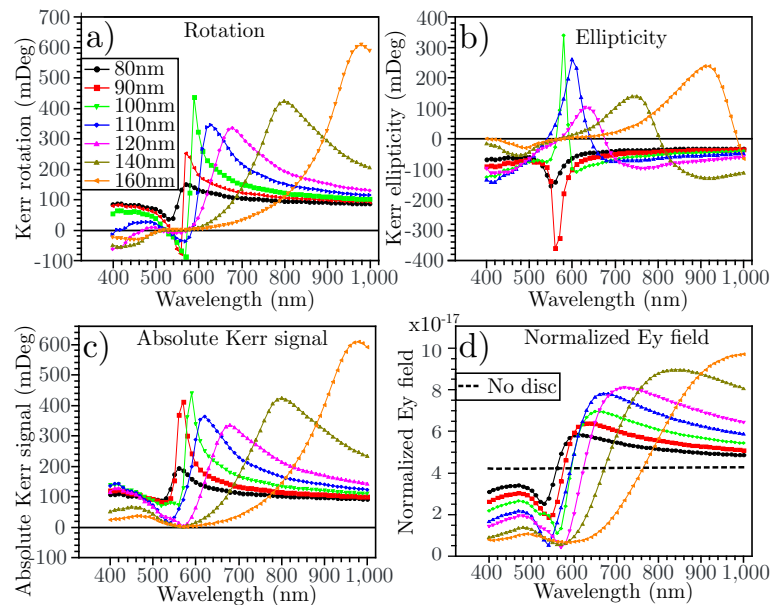
Fig. 6. Wavelength-dependent MOKE response for gold discs of different diameter (diameters are indicated in the legend). The discs were located 20 nm from the magnetic layer, and centered within the unit cell of the periodic model. (a) Kerr rotation, and (b) ellipticity. (c) The absolute Kerr signal (the sum of the rotation and ellipticity in quadrature) serves as a useful figure of merit, since the interplay between rotation and ellipticity is complicated. (d) Shows the reflected y component of the electric field normalized to the incident field amplitude (linearly polarized along the x axis with an amplitude of 1 V/m). This serves as a figure of merit when considering the practical implications of measuring the MOKE signal, and is comparable to the figure of merit derived in [4]. The dashed line in (d) shows the response of the model in the absence of a gold disc. The magnetic material modeled is the same as in the planar models without gold discs, and as such even the smallest resonance shown represents an enhancement of the MOKE signal on resonance.

The magnetic layer was defined as in previous models, and in the absence of an antenna gave polar Kerr rotation and ellipticity of $\approx$ 75 mDeg, and $\approx$ −25 mDeg respectively. Here it is useful to introduce an "absolute" Kerr signal, which is the rotation and ellipticity summed in quadrature. All discs show an enhancement of the absolute Kerr signal at resonance, from a modest increase for a diameter of 80 nm, up to an eight fold increase for the 160 nm diameter gold disc see Fig. 6. This increased Kerr response is likely due to the localized electric field enhancement near the gold disc at resonance, and hence increased electric field interaction with the magneto-optically active material below. The general trend of increasing resonant Kerr signal with increasing disc size is likely due to the increased area of interaction between this enhanced near field and the magnetic layer.The form of the resonance curve follows a similar pattern for all modeled antennas (including others not presented here) in that one component of the Kerr signal (rotation or ellipticity) exhibits a bi-polar variation, while the other exhibits a uni-polar behavior. A transition between two regimes was seen to occur at a diameter close to 100 nm, and so additional calculations were performed with diameters close to this value in order to gain further insight, these have been included in Fig. 6 as the 90 nm and 110 nm diameter curves. As can be seen in Fig. 6(b) the sign of the ellipticity signal changes for a disk diameter between 90 nm and 100 nm, while the rotation signal (Fig. 6(a)) exhibits a sharpened bi-polar form in this region. The resonances in both the rotation and ellipticity signals are observed to become broader as the diameter is detuned from the value at which the transition occurs. For disc diameters greater

than 110 nm, both rotation and ellipticity exhibit a uni-polar peak that increases in height with increasing disc diameter. Again this trend might be attributed to the increased area of interaction between the larger discs and the magnetic layer. However, closer study of the field distribution around the discs suggests that the electric field surrounding the larger discs in fact penetrates further into the magnetic layer. This latter effect does not fully explain the transition observed for disc diameters close to 100 nm. In order to explore the relationship between penetration depth and enhancement of the MOKE, a series of models were run, with a fixed disc diameter and varying distance between the gold disc and the magnetic layer. The results are summarized in Fig. 7 and reveal a correlation between distance and the size of the absolute Kerr signal, with the absolute Kerr signal decreasing as the disc is moved away from the magnetic layer. This lends further support to the hypothesis that the Kerr signal is enhanced due to an increase in the electric field within the magnetic layer. In addition to the trend in the absolute signal, we see a narrowing of the resonances as the distance is reduced. A dramatic change occurs when the separation reaches 10 nm. Here the Kerr rotation is greatly increased, with a peak absolute Kerr enhancement of $\approx 27\times$, while the resonance also narrows.
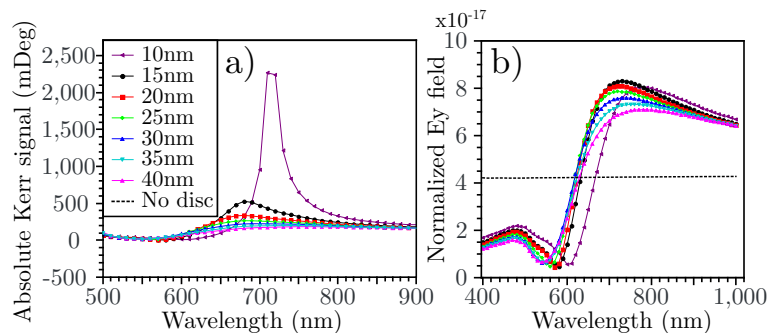

Fig. 7. Wavelength dependence of magneto-optical response for a gold disc of 120 nm diameter diameter placed at different distances from the magnetic layer (the separation between the gold disc and magnetic layer is indicated in the legend). (a) Shows the absolute Kerr rotation, and (b) shows the absolute y component of the normalized electric field. For clarity, data for the small smallest wavelengths has been omitted, since these showed behavior most likely associated with the periodicity of the model rather than the particle/under-layer separation.

A finer exploration of the parameter space around the separation yielding the largest Kerr signal was performed, Fig. 8. Here we observe a maximal Kerr response for the system with a 9 nm separation, and a rapid fall off in signal either side of this separation. We also see lengthening of the resonant wavelength with decreasing distance. This did not appear to occur for models with larger separations, which showed little change in the resonant wavelength as a function of changing separation. It should be noted that separations of < 10 *nm* may be realised for an antenna defined on the tip of an atomic force microscope probe [29].
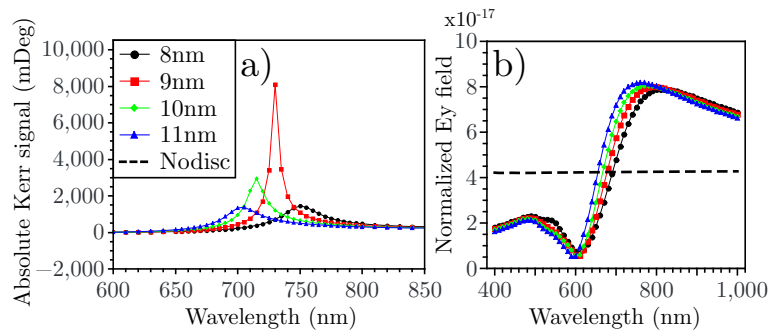
Fig. 8. Wavelength dependence of magneto optical response for a gold disc of 120 nm diameter diameter placed at different distances from the magnetic layer (again separation between the gold disc and magnetic layer is indicated in the legend). The spacing has been changed in finer steps around the value that showed the largest MOKE response in Fig. 7. As in the previous figure, (a) shows the absolute Kerr signal and (b) the normalized amplitude of the back reflected y component of the electric field. Here we see the maximum Kerr signal for a 9 nm gap, with a fall off in signal for gaps larger or smaller than this value. In addition, around 9 nm separation the resonant wavelength depends upon spacing, which was not observed for models with separations larger than 15 nm.

In order to provide insight into the spectra produced by different separations, Fig. 9 shows a comparison of the electric field distribution around the antenna, for a 40 nm separation, and the 9 nm separation that yields the largest Kerr signal. Note the field around the antenna appears to induce a higher field in the magnetic layer for the 9 nm separation. In addition the 40 nm separation shows a relatively symmetric field around the antenna, whereas for the 9 nm separation the field is concentrated on the side of the disc which faces the magnetic material. At the optimal separation a Kerr signal of over 8000 mDeg is observed, this represents a more then 100 fold increase of the $\approx$ 75 mDeg response of the magnetic film alone. To the best knowledge of the authors, this enhancement represents the largest increase in MOKE signal predicted for a system in which the magnetic material has not been altered. However due to the comparatively small values of the back reflected x and y components of the electric field, this mode would not necessarily provide large signal amplitude in practical experiments. It should also be noted that the magnitude of the observed MOKE signal is the quantity most sensitive to the detailed implementation of the model. Models with identical geometry but coarser mesh produce larger MOKE responses, while retaining the resonant wavelengths, than models with finer meshes. These models may therefore be better suited to predicting the conditions for resonance, rather than the size of the MOKE response.
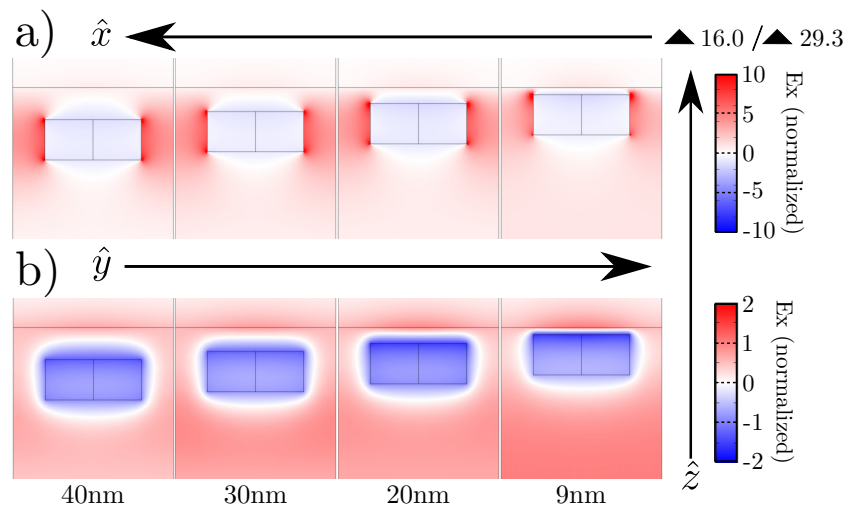
Fig. 9. Electric field distribution of a 120 nm diameter gold disc placed at distances of 40 nm, 30 nm, 20 nm, and 9 nm from the magnetic material. The cross-sections show the x component of local field, normalized by the incident field amplitude, plotted at one instance in phase. a) The field distribution for a cross section through the center of the $\hat{z}$, $\hat{x}$ plane. For clarity the color scale is limited to a maximum of 10 in the positive direction, the peak values are 16.0 for the 40 nm separation, and 29.3 for the 9 nm separation. b) The field distribution for a cross section through the center of the $\hat{z}$, $\hat{y}$ plane. The field appears to penetrate further into the magnetic layer for the case of 9 nm separation, which can be most clearly seen in the comparison of the $\hat{z}$, $\hat{y}$ plane field distribution.

Clearly the observed behavior is very sensitive to both the geometry of the disc, and it's separation from the sample. From the exploration of the parameter space reported here, two important relationships have been determined that might guide magneto-optical plasmonic antenna design. Firstly, the disc size has a strong influence upon the resonant wavelength, and some influence on the size of the enhancement at resonance, with larger discs producing (generally) larger magneto-optical response. Secondly, the separation between the antenna and the magnetic layer has a significant influence upon the size of the absolute Kerr response, and shape of the rotation and ellipticity spectra. By manipulating these two basic parameters it should be possible to tune an antenna to a desired wavelength, and then maximize the observed Kerr signal by positioning it sufficiently close to the magnetic material.

4. Conclusion

It has been demonstrated that the MOKE signal from a magnetic film may be calculated using commercially available finite element modelling software. The calculations have been shown to be robust, and, through appropriate choice of geometry and boundary conditions, both the polar and longitudinal MOKE response of a planar system can be determined. The rotation and ellipticity values calculated by the finite element method agree with analytical results for a semi-infinite medium to within 1 mDeg, or 2% the total for the material parameters used here. In addition the introduction of a gold nano-disc leads to a wavelength dependent resonance in the calculated MOKE signal. The signal at resonance is enhanced by a factor that depends upon the diameter of the disc and its separation from the magnetic material, and in some cases can reach a factor of over 100 times the magneto-optical response of the planar film in the absence of the disc. This platform allows one to model plasmonic resonators of more complicated geometry and composition, and their interaction with magneto-optically active materials. This work will

influence future probe design, and may lead to a probe capable of more sensitive or higher resolution magneto-optical imaging through combination with the platform developed in [29] Keatley et al. Such probes will be of increasing importance as magnetic and spintronic devices exploit magnetization dynamics that occur on length scales less than 100 nm and on time-scales within the pico-second regime.

5. Data access statement

The research materials supporting this publication can be publicly accessed in the open research Exeter (ORE) repository via the following persistent identifier: https://doi.org/10.24378/exe.104

Funding